INSTITUTE OF PLASMA PHYSICS

NAGOYA UNIVERSITY

A STUDY OF REVERSED FIELD PINCH EXPERIMENTS USING A NEW PROGRAMMING MODE

Y. Kita

(Received Aug. 10, 1979)

IPPJ- 415 Aug. 1979

RESEARCH REPORT

NAGOYA, JAPAN

A STUDY OF REVERSED FIELD PINCH EXPERIMENTS USING A NEW PROGRAMMING MODE

Y. Kita

(Received Aug. 10, 1979)

IPPJ- 415 Aug. 1979

Further communication about this report is to be sent to the Research Information Center, Institute of Plasma Physics, Nagoya University, Nagoya 464, Japan.

ABSTRACT

A new mode of external-field programming for setting up a reversed-field pinch (RFP) is tested in STP-1. It involves creating an initial plasma with a screw pinch followed by external-field reversal. The program is done carefully so as to satisfy the equilibrium relation with respect to the minor radius throughout the setting-up phase. Increase of the trapped flux in the plasma by a factor of two is consequently attained, as compared with previous usual programming mode. Actually, at a plasma current of 58 kA, a stable operation time of 13 μsec is achieved with a density of 3.5×10^{15} cm^{-3} and a temperature of 20 eV. After 13 μsec stable operation time, the plasma is suddenly crashed down by a violent MHD instability. One dimensional stability analysis based on ideal MHD model is applied to the experimental results. It is found that the instability is $m = 1$ resistive tearing mode under the influence of viscosity. Using the new programming high current operation at 110 kA is done and results in higher plasma temperature and density of 40 eV and 4.5×10^{15} cm^{-3}, respectively. The duration of stable discharge, however, is limited to about 10 μsec, in spite of the expected longer confinement time at the higher temperature.

1. INTRODUCTION

Studies of a high β plasma confinement are important to achieve economic fusion reactor since its output power scales with square of β value. The reversed-field pinch (RFP) has been received much attention as one of possible methods to obtain a high β toroidal plasma. As is known in RFP, the plasma stability relays on high magnetic shear which is produced by reversed toroidal field outside the plasma. Theoretical prediction tells that RFP can be stable up to β of 0.3 with the aid of a conducting copper shell.[1] It is also expected that RFP may have a big advantage over tokamak since high joule heating current is achieved above Kruscal-Shafranov limit enough to get ignition. In the original RFP experiment of Zeta,[2] stable RFP configuration is created spontaneously by an unstable plasma motion itself. In recent experiments,[3-6] however, it is often produced by rapid field programming for avoiding strong plasma-wall interaction caused by necessary unstable plasma motion for setting up in spontaneous way. Thus it becomes important in the programmed RFP to control the field in order to maintain plasma equilibrium and stability in the setting-up phase. In section 3 a new field programming is described, in which the above-mentioned factors are taken into account. In section 4, a study of MHD instability which destroys a stable RFP discharge is given. In order to study the basic property of this instability, one dimensional ideal MHD stability analysis[7] is done. The results are compared with observed various quantities originating from the instability. High current operation is examined in section 5, whose current density of 4 $kA \cdot cm^{-2}$ is an interesting one for a compact ohmically heated RFP reactor.[8] A reactor study pointed out that the plasma diameter necessary for RFP reactor scales sensitively with the plasma current density. It is calculated that the current density required for a

compact RFP reactor must exceed 3 $kA \cdot cm^{-2}$.

2. EXPERIMENTAL SET-UP

As can be seen from the schematic drawing of Fig.1, STP-1 is small but the design exhibits a high degree of flexibility. The quartz torus has a major and a minor radius of 12 cm and 4.2 cm, respectively. The inner radius of the copper shell is 4.75 cm. Attached power crowbar systems for both θ- and z-circuits with extremely low leakage inductance transformer make it possible to program a variety of fields.[9] Measurements of plasma current I_p, toroidal magnetic field at the wall B_e and total magnetic flux inside copper shell Φ_t are obtained by Rogowskii coil and one-turn loop winded around the minor radius of the shell. Three vector components of toroidal (B_t), poloidal (B_p) and radial field (B_r) are observed by small four pick-up coil inserted into plasma. Electron line density along vertical direction is measured by He-Ne laser Michelson interferometer. In our experiment low- and high-current operations are examined. The time sequences are given in Fig.2. Deuterium gas is introduced into the discharge tube through a fast acting gas valve. The initial gas pressure in the tube is varied from 1.7×10^{-2} torr to 6.0×10^{-2} torr. Electron gun is used to help the break-down of the filling gas. Pre-ionization is made by stabilized z-pinch. Further ionization and pre-heating are accomplished by screw pinch. The main parameters of STP-1 are listed in Table 1. Figure 3 shows typical wave forms of I_p, B_e and Φ_t in low-current operation. When a RFP-field is set up, the peak plasma current and the average peak current density are 58 kA and 2 $kA \cdot cm^{-2}$, respectively. After the maximum current is attained, crowbar timing of I_p is purposely delayed for 5 μsec in order to avoid the increase of pinch-ratio θ. On the other hand the peak plasma current and the average

peak current density of high current operation are 110 kA and 4 kA·cm^{-2}, respectively. The typical waveforms of I_p, B_e and Φ_t in high current operation are shown in Fig.4.

3. EXPERIMENTAL RESULTS AND DISCUSSION OF NEWLY PROPOSED OPERATION

STP-1 has been operated with three different programming modes, including the newly proposed one (S-mode) in addition to the two previously studied ones (C-mode and M-mode). Typical time sequences of these different programming modes are shown in Fig.5. The present S-mode is carefully programmed for plasma to satisfy the equilibrium relation during both screw pinch and reversed-field setting-up phase. The equilibrium relation,

$$B_p^2 + B_e^2 = 2\mu_0 \langle P \rangle + \langle B_i^2 \rangle \qquad (1)$$

where B_e is external toroidal field, B_p poloidal one, B_i internal toroidal one and P is plasma pressure. Actual waveforms of I_p, B_e and Φ_t are shown in Fig.3. Pre-ionization is made by stabilized z-pinch in toroidal bias field of 0.48 kG and maximum plasma current of 18 kA by which ionization rate reaches up to 0.6-0.7. Further ionization and pre-heating are accomplished by screw-pinch where toroidal field rises from 0.48 kG to 4.5 kG and plasma current I_p reaches 28 kA in 2.4 μsec and thus fully ionized plasma ready for RFP-field programming is created. In the screw pinch phase radial oscillation is observed. Figure 6 shows time evolution of toroidal field distribution across the plasma normalized by the vacuum field. Due to radial oscillation the plasma shows pra- and dia-magnetism alternatively, which indicate that high density plasma is well developed.[10] To produce RFP configuration, toroidal field at the wall is reversed while plasma

current I_p is continued to increase from 28 kA up to 58 kA during the field reversal. The increase of the plasma current is necessary by about factor two during the programming for field reversal without violating the equilibrium relation. As can be seen in Fig.7 which shows time evolution of B_p and B_t field profiles, it appears that the expansion of the plasma column caused by decrease of B_t at the wall is compensated by increase of plasma current which generates poloidal field. We mention here that in recent study on HβTX-1 experiment in Culham the programming which starts with screw pinch is also described.[11] However, in Culham case plasma current is not increased while toroidal field is reversed, which may violate the plasma equilibrium during RFP setting-up. As is seen in Fig.8, we found that the present operation has a definite advantage over the C-mode operation tested in STP-1 since toroidal trapped flux of the present mode is larger by factor two compared with the one of C-mode. The curves in Fig.8 are obtained under the restriction of the same charge-up voltage to the capacitor to induce plamsa current. The other parameters like bias field or program timing are varied so as to maximize toroidal trapped flux. We believe that this big difference arises from high ionization degree and temperature due to screw pinch, which is also effective to induce larger plasma current in the present mode. The F, θ diagram[12] of the present operation is given in Fig.9. In the present mode θ value can be set to be less than 2 when RFP is set up, while in Culham mode operation in STP-1 it is impossible to make it less than 2 because of insufficient trapping of toroidal flux in the plasma. Figure 8(A) shows the field distribution of the present new operation when RFP configuration is set up. The dotted line shows pressure profile deduced by the field profiles on the assumption of MHD equilibrium with toroidal effect taken into account.[13] Beta poloidal β_p estimated from the pressure profile is 0.52. The arrow in Fig.8(A) displays the position of magnetic

axis estimated from Shafranov's formula;

$$\Delta/b = -\frac{b}{2R}\{\ell n(b/a) + (\beta_p + \frac{\ell_i}{2} - \frac{1}{2})(1 - (\frac{a}{b})^2)\} \qquad (2)$$

where Δ is the displacement of the magnetic axis from the center of the discharge tube, a plasma radius, b shell radius, ℓ_i internal inductance, and R is major radius. Coincidence of the magnetic axis calculated from Shafranov's formula with the one measured by magnetic probes may be one of good evidences that plasma is in equilibrium. With the aid of line density measurement by He-Ne interferometer, plasma temperature can also be estimated from the value of plasma pressure. The equality of electron and ion temperature may be expected, since electron-ion energy equipertition time is calculated to be about 0.4 μsec while e-folding time of ion energy loss due to thermal conduction is about 1.2 μsec for the parameter range interesting here. The plasma temperature thus estimated is found to be 20 eV when RFP is set up. The hollow pressure profile is preferable for stability and β_p value of 0.52 satisfies the stability condition for m = 0 mode. Actually one dimensional ideal MHD stability analysis is done for the field profiles of Fig.8(A) using a computer code used in Ref.7. It is found that the plasma should be stable for m = 0 mode but unstable mode exists for m = 1 provided that stability analysis of straight cylinder is also applicable to fat STP-1 system. In order to treat the toroidal effect simply, we assume that center of each magnetic surface concentrates on the axis of the cylinder. Figure 10 shows the corrected field profile after the above manner. Small displacement ξ_r distribution for m = 1, k = -8.0 mode, which gives largest growth rate, is also given in the same figure. Calculated growth rate for m = 1 mode is shown in Fig.11 curve (A) as a function of wave number k of toroidal direction. If m = 1 mode is active, B_r component of

the field should appear. However in the experiment B_r signal is not apparent at the time when RFP is just created. The reason why B_r is not clearly observed may be believed that B_r is related to with equation,

$$B_r - i\,(mB_p/r - kB_t)\,\xi_r = 0 \qquad (3)$$

where in the present case ξ_r is localized near singular point, so that the term in the bracket becomes zero. Although the preferable hollow pressure profile is maintained for only 2-3 μsec, plasma seems to be grossly stable for 13 μsec until the sharp dip of electron line density appears as is shown in Fig.3. It is found that the diffusion time of the trapped flux before the sudden dip of electron line density is not inconsistent with the classical process by a rough estimation neglecting external circuit.[14] If we use the experimental value of T_e = 20 eV and a_p (averaged plasma radius) = 2.3 cm, the classical diffusion time ($e = \mu\sigma a^2/(10\text{-}15)$) becomes 7.5-11.2 μsec, while the observed e-folding decay time τ_e of the trapped flux is 8.7 μsec, where σ denotes the plasma conductivity and the factor (10-15) depends on the different current distribution.[2] The appearance of the dip in Fig.3 is coincident with the time when θ value becomes larger than 2 as is shown in Fig.9.[15]

4. EXPERIMENTAL RESULTS AND DISCUSSION FOR THE INSTABILITY

As is clear from the measurement of electron line density in Fig.3, plasma is crashed down after the stable discharge time of 13 μsec. The appearance of this instability is coincident with the time when θ value becomes larger than 2 as is shown in Fig.9. In our case such instability appears at wide range of filling gas pressure. Figure 12 shows the relation

between averaged electron line density n_e and Δt where Δt is a time for the dip to reach its bottom as is illustrated in Fig.3. In order to study the instability further, a little larger reversed field is applied because it triggers much unstable plasma motion which may ease the observation of detail structure of the instability. Typical waveforms of enhanced reversed-field operation are shown in Fig.13. Measurement of electron line density at center of the tube along vertical direction and B_r at 2.5 cm from the tube center are also done and their results are given in Figs.14(A), (B) respectively. As is seen in B_r signal, a hump followed by density dip appears in 20 to 26 μsec. The distributions of B_p, B_t and P at the time (21 μsec) just after the start of the instability are shown in Fig.15. In this figure there appears a peaking of plasma pressure which may be caused by peaking of plasma current. According to reference (16), an ideal MHD calculation may be valid for a study of B_r profile except near the singular point where resistivity becomes very important. We can see in reference (16) several examples of stability calculations based on Force Free Bessel Function and Pitch Pressure model in which resistivity and viscosity are taken into account. The MHD stability calculation is also done for this profiles of Fig.15 in order to know whether observed B_r profile can be explained from the ideal MHD calculation. As a result the calculation shows that the profile is stable for m = 0 mode but is unstable for m = 1 mode, calculated growth rate of which is given by the curve (B) of Fig.11. Figure 16 shows the corrected field and pressure profiles after Fig.15 and calculated ξ_r and B_r distributions for m = 1, k = - 2.8 mode. We choose k = - 2.8 since it gives largest calculated growth rate. As is seen in Fig.16 ξ_r and B_r are localized at the central region where Suydam condition[17] is violated because of the peaking of plasma pressure. The dotted curve in Fig.17 shows observed B_r signal distributions over plasma radius

at 19, 20, 21, 22 μsec after the start of discharge. The solid line shows the calculated B_r profile at 21 μsec. The B_r profile has approximate similarity to the observed one in the sense that both profiles are peaked at the center. However they do not coincide around the singular point. If resistivity is included, the term $\sigma^{-1}\Delta B_r$ should be added to eq.(3), where σ is electrical conductivity and Δ is Laplacian operater. Therefore B_r may not be zero at the singular point. Actually we can see an example[16] of calculation of B_r profile for low magnetic Raynols' number ($s \sim 100$) where B_r is peaked at the center but not zero near the singular point. So this mode may be supposed to be m = 1 resistive tearing instability which is influenced by resistive effect especially at singular point. Calculated growth rate of 1.5-2.6 x 10^6 sec^{-1} does not agree with the observed growth rate of 6.7 x 10^6 sec^{-1} attained from the time evolution of B_r but the former is larger by factor 2-4 than the latter. The reduction of the growth rate is considered to come from viscosity effect. According to calculation also in Ref.16 where viscosity is included, the growth rate is found to be diminished by about factor 2 compared with ideal MHD case when S value is as low as 100 like the present case. Therefore the instability which we are facing now, may be m = 1 resistive tearing mode partially influenced by viscosity. Figure 14 (C) shows time evolution of the growth rate calculated with measured equilibrium fields and pressure profile. The growth rate becomes larger and larger as the discharge proceeds, since the plasma current density gradually peakes around the magnetic axis until the current profile is flattened out by the instability. The increase of the growth rate is followed by a hump of B_r signal and a breaking of Φ_t curve as is seen in Fig.14(A). The toroidal flux is generated by the poloidal component of a plasma current and also by an external coil current. Since external coil current is quite smooth in the present case, the existence of the

breaking point on the curve should show that the instability is closely related to the sudden flux change which is originated by an unstable helical plasma current motion.[18] In particular at low filling gas pressure operation of 1.7×10^{-2} torr Φ_t curve shows even a hump as in Fig.13(B). In this case it can be said that the considerable amount of positive toroidal flux is generated by the instability.

5. HIGH CURRENT OPERATION

In the low current operation plasma becomes unstable when the pinch ratio θ exceeds 2. The θ value gradually increases with the diffusion of toroidal flux Φ_t trapped in the plasma until the instability occurs. The diffusion time of the trapped flux is not inconsistent with the time estimated under the classical process. If the temperature of the initial plasma is further improved and the increase of θ value is further reduced, we could expect longer stable discharge time. Therefore, we increase the plasma current density by about factor two, expecting to achieve a higher plasma temperature and a longer confinement time. The typical plasma current when the reversed field is set up is now 110 kA, which gives average and maximum current density of 4 kA·cm^{-2} and 6 kA·cm^{-2}, respectively. The characteristic behavior of B_e, Φ_t and I_p is shown in Fig.4. The He-Ne laser interferometer output and the soft X-ray as detected by a pin-diode are also shown in this figure. Compared with the low current density case the electron density becomes 3.2 times as high as is expected from the filling pressure. The same phenomenon is described in Ref.19. Figure 18 shows typical profiles of B_t and B_p fields for high-current operation at the instant when the reversed field is set up; the dotted line gives the pressure distribution obtained with the same manner. The average electron

line density and the electron temperature derived from plasma pressure and electron line density are 7.5 x 10^{15}·cm^{-3} and 40 eV, respectively. The poloidal beta β_p is estimated to be 0.48. The observed position of the magnetic axis agrees fairly well with that given by the Shafranov's formula. Also, the plasma becomes highly unstable to m = 1 mode at 10 μsec after the set-up of the reversed configuration. But the value of β_p just before the instability is about 0.8, which satisfies the stability condition for m = 1 ideal MHD mode. A sudden dip of the He-Ne interferometer line density is also observed with the instability. It should be noted that in high current operation the one-turn voltage waveform becomes ragged and many spikes appear while those spikes are flattened out if the peak current is reduced to 90 kA as shown in Fig.19. Another particular feature of the high-current case is the appearance of a strong X-ray signal burst which lasts up to the time where Φ_t is reversed. However, in spite of the apparent improvement of the plasma temperature, plasma is crashed down by the instability and stable discharge time is not extend. These may be caused by the current peaking deduced from the cooling effect near the plasma surface through the increased plasma-wall interaction. The plasma-wall interaction may be enhanced by the higher MHD activities as is seen in Fig.19.

6. CONCLUSION

Using newly proposed mode, RFP configuration is set up and trapping of toroidal flux is improved by factor 2 compared with the commonly used previous program. The RFP plasma thus created, has a hollow pressure profile which is preferable for stability. However the plasma column is destroyed by strong instability caused by the peaking of plasma current at the center of plasma at 13 μsec later after the RFP is set up. It is found

the principal mode of the instability may be m = 1 resistive tearing mode influenced by viscosity. The measured growth rate is observed to be 2 to 4 times smaller than the one calculated with pure MHD model. We suppose that the viscosity may reduce the growth rate.[16] It can be said that the change of Φ_t with the instability is closely related to unstable helical plasma current motion. In our case the change of Φ_t is especially remarkable at operation of low filling gas pressure. Just after RFP is set up, MHD unstable singular point is yielded localizing near the surface of the plasma. The existence of unstable region at the plasma surface may contribute to the peaking of the plasma current. Using the same mode, high current density operation is also done expecting more longer stable discharge time because of the higher temperature. However, in spite of apparent improvement of the temperature, stable discharge time is not extended, perhaps because of the raised level of MHD activities which may induce a larger trapped flux loss.

Acknowledgements

The author would like to express sincere gratitude to Professor K. Hirano for his guidance during the course of this work. He is also indebted to Professors H. Oshiyama and M. Wakatani and Dr. S. Kitagawa for their useful advice and helpful discussion. He acknowledges Mrs. S. Yamada, Mr. T. Kato, Mr. K. Kawamura and Mr. T. Naito for the technical assistance.

APPENDIX: STABILITY OF RFP

Stability of RFP has been investigated during these twenty years. Some recent studies[7,16] include resistivity and viscosity. In this section, however, descriptions are restricted to ideal MHD theory sicne ideal MHD stability analysis is used in this paper. Within ideal MHD theory, stability of a system is described by Newcomb's criterion which is powerful method based on the hydromagnetic energy principle. When the equilibrium configuration of the system does not satisfy the Newcomb's criterion, MHD kink instability may occur. In order to calculate the growth rate and radial magnetic field B_r distribution of the instability, we use the following formation. The basic equations describing an ideal MHD plasma state are

$$\rho \frac{d\vec{v}}{dt} = - \text{grad } p + \vec{J} \times \vec{B} , \tag{A-1}$$

$$\frac{\partial \rho}{\partial t} + \text{div}(\rho \vec{v}) = 0 , \tag{A-2}$$

$$\vec{E} + \vec{v} \times \vec{B} = 0 , \tag{A-3}$$

$$\frac{d}{dt} (p\rho^{-\gamma}) = 0 , \tag{A-4}$$

$$\text{rot } \vec{E} = - \frac{\partial \vec{B}}{\partial t} , \tag{A-5}$$

$$\text{rot } \vec{B} = \vec{J} , \tag{A-6}$$

$$\text{div } \vec{B} = 0 . \tag{A-7}$$

Let $\vec{E}$ be the electric field, $\vec{B}$ the magnetic field, $\vec{J}$ the current density,

ρ the mass density, p the pressure, γ the ratio of specific heat and $\vec{v}$ the fluid velocity. These equations are written in rationalized Gaussian unit with $c = 1$. Mathematically the problem of stability is reduced to the investigation of small perturbations about an equilibrium state. If the perturbation amplitudes are small, the linealized equations of motion may be used. Let $\tilde{\rho}$, $\tilde{p}$ and $\vec{b}$ represent small deviations from the equilibrium value ρ, p and $\vec{B}$. The equations describing the static equilibrium are derived from eqs.(A-1)-(A-7):

$$\vec{J} \times \vec{B} = \text{grad } p \ , \tag{A-8}$$

$$\text{rot } \vec{B} = \vec{J} \ , \tag{A-9}$$

$$\text{div } \vec{B} = 0 \ . \tag{A-10}$$

The linearized equations of eqs.(A-1)-(A-7) can be written in the form:

$$\frac{\partial \tilde{\rho}}{\partial t} + \text{div } (\rho \vec{v}) = 0 \ , \tag{A-11}$$

$$\rho \frac{\partial \vec{v}}{\partial t} + \text{grad } \tilde{p} = \text{rot } \vec{B} \times \vec{b} + \text{rot } \vec{b} \times \vec{B} \ , \tag{A-12}$$

$$\frac{\partial \tilde{p}}{\partial t} + \vec{v} \ \text{grad } p + \gamma p \ \text{div } \vec{v} = 0 \ , \tag{A-13}$$

$$\frac{\partial \vec{b}}{\partial t} = \text{rot } (\vec{v} \times \vec{B}) \ . \tag{A-14}$$

Since it is not always convenient to use the velocity $\vec{v}$, we treat the displacement ξ from an equilibrium position, under the condition of $\vec{v} = \partial \vec{\xi}/\partial t$. Using this ξ, eqs.(A-11), (A-13) and (A-14) can be integrated with respect

to time as

$$\tilde{\rho} = - \operatorname{div} (\rho \vec{\xi}) \ , \tag{A-15}$$

$$\tilde{p} = - \vec{\xi} \operatorname{grad} p - \gamma p \operatorname{div} \vec{\xi} \ , \tag{A-16}$$

$$\vec{b} = \operatorname{rot} (\vec{\xi} \times \vec{B}) \ . \tag{A-17}$$

Substitution of these expressions into eq.(A-12) results in a single second order differential equation of the form,

$$\rho \frac{\partial^2 \vec{\xi}}{\partial t^2} = \vec{F} \{\vec{\xi}\} = \operatorname{grad} (\vec{\xi} \operatorname{grad} p + \gamma p \operatorname{div} \vec{\xi})$$

$$+ \operatorname{rot} \vec{B} \times \operatorname{rot} (\vec{\xi} \times \vec{B})$$

$$+ \operatorname{rot}[\operatorname{rot}(\vec{\xi} \times \vec{B})] \times \vec{B} \ . \tag{A-18}$$

In order to calculate the growth rate and B_r profile, we introduce cylindrical coordinate r, θ, z about the axis of symmetry. The pressure, the density, and the magnetic field is assumed to be an only function of r. The field component B_r vanishes and the components B_θ and B_z depend only on r. The current density in the plasma is determined by Maxwell's equation (A-6); the radial component J_r therefore vanishes and the other components are given by

$$J_\theta = - \frac{dB_z}{dr} \ , \qquad J_z = \frac{1}{r} \frac{d}{dr} (rB_\theta) \ .$$

Since the configuration for the stability to be tested must be in equilibrium state, radial distribution of the plasma pressure p must be governed by the MHD equilibrium equation (A-8), which reduce to

$$\frac{dp}{dr} + B_z \frac{dB_z}{dr} + \frac{B_\theta}{r} \frac{d}{dr} (rB_\theta) = 0 \ .$$

Starting from eq.(A-18) and taking normal mode solutions

$$\vec{\xi} = (\xi_r(r), \xi_\theta(r), \xi_z(r))e^{\omega t+im\theta-ikz} \ ,$$

We obtain three coupled equations:

$$\omega^2\rho\mu/r \qquad\qquad (-P^2/r - 2B_\theta(\frac{B_\theta}{r})'/r)\ \mu$$

$$i\omega^2\rho(rB_\theta\eta - kr\zeta)/(mB_\theta - krB_z) \quad = \quad -i(2kB_\theta B_z/r^2)\ \mu$$

$$i\omega^2\rho(m\zeta - rBz\eta)/(mB_\theta - krB_z) \qquad i(2kB_\theta{}^2/r^2)\ \mu$$

$$+ ((\gamma p/r + B^2/r)\mu')' + \gamma(p\eta)'$$

$$+ \{(kB_\Theta + mB_z/r)\zeta\}' + 2(kB_\theta/r)\zeta \qquad \text{(A-19.a)}$$

$$+ i(\gamma mp/r^2 + B_z(mB_z/r + kB_\theta)/r)\mu'$$

$$+ i(\gamma mp/r)\eta + i((k^2 + m^2/r^2)B_z)\zeta \qquad \text{(A-19.b)}$$

$$- i(\gamma kp/r + B_\theta(mB_z/r + kB_\theta)/r)\mu'$$

$$- i\gamma kp\eta - i\{(k^2 + m^2/r^2)B_\theta)\zeta \qquad \text{(A-19.c)}$$

where we have used the variables $\mu = r\xi$, η, ζ and accents mark denotes differentiation with respect to r. η and ζ are defined as the following equations,

$$\eta = \vec{\nabla}\cdot\vec{\xi} - \frac{1}{r}\frac{d}{dr}(r\xi_r) = \frac{im}{r}\xi_\theta - ik\xi_z ,$$

$$\zeta = i(\vec{\xi} \times \vec{B})_z = i\xi_\theta R_z - i\xi_z B_\theta .$$

From eqs.(A-19.b) and (A-19.c) we can derive

$$\eta = (2kB_\theta\omega^2\rho(kB_\theta + mB_z/r)/Nr^2)\ \mu$$

$$- \{(\gamma pG(\omega^2\rho + F^2) - \omega^2\rho(kB_\theta + mB_s/r)^2)/Nr\}\mu' \qquad (A\text{-}20)$$

and

$$\zeta = (2kB_\theta(\omega^2\rho B + \gamma pF^2)/Nr^2)\ \mu$$

$$- \{(kB_\theta + mB_s/r)(\gamma pF^2 + \omega^2\rho(\gamma p + B^2))/Nr\}\mu' , \qquad (A\text{-}21)$$

where

$$N = \omega^4\rho^2 + \omega^2\rho G(\gamma p + B^2) + G\gamma pF^2,$$

$$F = mB_\theta/r - kB_z$$

and

$$G = k^2 + m^2/r^2$$

Equation (A-19.a) can be rewritten as

$$- \{(\omega^2\rho + F^2 + 2B_\theta(B_\theta/r)')/r\}\mu + [\{(\gamma p + B^2)/r\}\mu' + \gamma p\eta$$

$$+ (kB_\theta + mB_z/r)\zeta]' + (2kB_\theta/r)\zeta = 0. \qquad (A\text{-}22)$$

Substitutions of eqs.(A-20) and (A-21) into eq.(A-22) make the final form of the equation to be solved as

$$\left[\frac{(\omega^2\rho + F^2)\{\omega^2\rho(\gamma p + B^2) + \gamma\rho F^2\}}{N} \cdot \frac{1}{r}(r\xi)'\right]'$$

$$+ \left[-\omega^2\rho - F^2 - 2B_\theta\left(\frac{B_\theta}{r}\right)' + \frac{4k^2B_\theta^2}{r}\,\frac{\rho\omega^2B^2 + \gamma\rho F^2}{N}\right.$$

$$\left. + r\left\{\frac{2kB_\theta(mB_z/r + kB_\theta)}{r^2}\;\frac{\rho\omega^2(\gamma p + B^2) + \gamma\rho F^2}{N}\right\}'\right]\xi = 0 \,, \qquad \text{(A-23)}$$

where we have used the relation $\mu = r\xi$ and ω is the growth rate. The growth rate γ and B_r profile are obtained by solving the equation of motion for r direction (A-18) under the following boundary conditions. They are:

$$r\xi = 0 \quad \text{at} \quad r = 0 \,,$$

ξ is relation with ψ given by eq.(A-24) at $r = a$, and $\psi = 0$ at $r = b$, where a and b denote the radius of the plasma column and of the conducting shell respectively. Here eq.(A-24) is

$$\psi = (nkrB_z - mB_\theta)\;\xi_r/r \,, \qquad \text{(A-24)}$$

In practical estimation, $B_\theta(r)$, $B_z(r)$, $p(r)$ and ρ are experimentally given. The growth rate of the instability is obtained by choosing ω which gives $\xi_r(r)$ for the boundary condition to be satisfied.

REFERENCES

1. D.C. Robinson, Plasma Phys. 13 (1971) 439
2. H.A.B. Bodin, 3rd Topical Conf. Pulsed High Beta Plasma, Culham, B1,1,39 (1975).
3. C.W. Gowers, D.C. Robinson, A. Sykes, A.J.L. Verhage, J.A. Wesson, M.R.C. Watt, H.A.B. Bodin, 6th Conf. on Plasma Physics and Controlled Nuclesr Fusion Research, Berchtesgaden, VI, 429 (1976).
4. D.A. Baker, L.C. Burkhardt, J.N. Di Marco, A. Haberstich, R.L. Hagenson, R.B. Howell, H.J. Karr, A.E. Schofield, ibid. VI, 419 (1976).
5. A. Buffa, S. Costa, R. Giannella, G. Malesani, G.F. Nalesso, S. Ortolani, ibid. VI, 447 (1976).
6. T.Shimada, Y.Hirano, Y.Maejima, K.Ogawa, ibid. VI, 463 (1976).
7. T.Amano, T.Tamai, M.Wakatani, J.Phys, Soc. Japan 32 (1972) 1385.
8. R.L.Hagenson, private communication. (1976).
9. S.Kitagawa, K.Hirano, Rev. Sci. Instrum. 45 (1974) 962.
10. M.Mimura, K.Hirano, J.Phys. Soc. Japan 42 (1977) 3234.
11. BUT, E.P., et al, 7th Europ. Conf., Lausanne P.39 (1975).
12. J.B.Taylor, in Plasma Physics and Controlled Nuclear Fusion Reseach (Proc. 5th Int. Conf. Tokyo, 1974) Vol. 1, Vienna (1975) 161.
13. M.Mimura, K.Hirano, Japan. J. Appl. Phys. 13 (1974) 1493.
14. A.J.L. Verhage, Culham Labaratory Report, CLM-R161 (1976).

15. E.P.Butt, C.W.Gowers, R.F.Gribble, A.N.Liyin, A.A.Newton, B.A.Norton, 5th Intern. Conf. on Plasma Physics and Controlled Nuclear Fusion Research, Tokyo, 417 (1974).

16. J.A.Dibiase, UCRL-51591 (1974).

17. B.R. Suydam, Proc. 2nd Intern. Conf. on Peaceful Uses of Atomic Energy, Genova, 31 (1958) 157.

18. A.J.L. Verhage, A.S.Furzer, D.C. Robinson, Culham Laboratory Preprint, CLM-P 463 (1976).

19. C.A.Bunting, et al., 8th Europ. Conf. Prague p.79 (1977).

FIGURE CAPTIONS

Fig.1. A schematic drawing of the STP-1 toroidal pinch discharge apparatus.

Fig.2. Typical time sequence of the newly developed RFP mode for low and high current operations.

Fig.3. Time evolutions of four plasma parameters for low current operation. (A) Typical waveforms of plasma current I_p, external field B_e and total magnetic flux Φ_t inside copper shell. (B) Time history of averaged electron line density observed by He-Ne interferometer with the light path at discharge tube center along vertical direction.

Fig.4. Time evolution of plasma parameters for high-current operation. (A) Waveforms of I_p, B_e and Φ_t. (B) Time history of electron line density of discharge tube center along z-axis. (C) Soft X-ray signal detected by pin diode.

Fig.5. Time sequences of three different RFP programming modes. Typical plasma current I_p and toroidal field B_e at the wall are illustrated. (A) C-mode studied in HBTX-1and ZT-S experiments at Culham and Los Alamos, respectively. (B) M-mode studied in Eta-Beta experiment. (C) S-mode tested in present STP-1 experiment. (1) Ionization and pre-heating phase; (2) screw-pinch phase; (3) setting-up phase of reversed configuration; (4) reversed phase.

Fig.6. Time evolution of toroidal field B_t distribution normalized by vacuum field at screw pinch phase. These distributions show para- and diamagnetism owing to radial oscillation. The time given on the figure is from the start of the discharge.

Fig.7. Time evolutions of B_t and B_p field distributions during RFP setting up phase after screw pinch.

Fig.8. Comparison of fields (solid line) and pressure (dotted line) distribution just after the RFP configuration is set up for two different modes studied in the same machine with the same charging voltage of capacitor bank for driving plasma current. (A) The profiles for B_t, B_p and P for the newly developed mode at 13 μsec after the start of the discharge with filling deuterium gas of 3.5×10^{-2} Torr. The arrows show magnetic axis position obtained from Shafranov's formula. (B) The profiles for the mode obtained by Culham mode with bias field of 1.75 kG and maximum plasma current of 42 kA and filling helium gas of 5.0×10^{-2} Torr.

Fig.9. Time evolution in F-θ diagram for low-current case. F is the field reversal ratio, $F = B_t$ (wall)$/B_t$ (average). θ is the pinch ratio, $\theta = B_p$ (wall)$/B_t$ (average). The numbers show the times used in Fig. .

Fig.10. (A) The profiles for B_t, B_p and P derived from the profiles of Fig.6(A) to be convenient for one dimensional ideal MHD stability analysis, assuming that the center of each magnetic surface is coincident with cylinder axis. Magnetic field is normalized by B_{tmax} and P is normalized by $B^2_{tmax}/2\mu_o$. μ_o is vacuum permeability and B_{tmax} is a maximum value of B_t. (B) The calculated distribution of small displacement ξ_r for the mode of m = 1, k = -0.8 for the profiles of the B_t, B_p and P in Fig.7(A).

Fig.11. Growth rate (γ) as a function of axial wavenumber k. (A) γ for the profiles of Fig.8(A). (B) γ for the profiles of Fig.14(A). γ is normalized by $B_{pmax}/a\sqrt{P_o}$, where a is plasma radius and P_o is plasma pressure at the center and B_{pmax} is maximum value of B_p.

Fig.12. Δt as a function of averaged electron line density $\bar{n}_e$ observed at discharge tube center along vertical direction. Δt is a time necessary for the dip to reach its bottom as is illustrated in Fig.3(B).

Fig.13. (A) Typical waveforms of I_p, B_e and Φ_t in the case of filling deuterium gas of 3.5×10^{-2} Torr and with more reversed field than Fig.3. (B) Typical waveforms of B_e and Φ_t in the case of filling deuterium gas of 1.7×10^{-2} Torr with the same maximum plasma current as the case in figure (A).

Fig.14. Time evolution for three parameters obtained from the operation given in Fig.11(A). (A) Averaged electron line density observed by He-Ne interferometer. (B) Radial magnetic field observed at 2.5 cm from center of discharge tube. (C) Growth rate for m = 1 mode calculated from the fields and pressure profiles with aid of one dimensional ideal MHD stability code.

Fig.15. Magnetic field components B_t and B_p as a function of radius as measured with magnetic probes at 21 μsec of Fig.11(A). The pressure profiles (solid line) are derived from the fields with aid of MHD equilibrium code.

Fig.16. (A) Time profiles for B_t, B_p and P derived from the profile of Fig.12 with the same manner as one in Fig.8(A). (B) The calculated distributions of ξ_r and B_r for the mode of m = 1 and k = -2.8 for B_t, P_p and P profiles of figure (A).

Fig.17. (A) Observed B_r signals as a function of radius at 19, 20, 21, 22 μsec from the start of the discharge. The solid line is B_r profile calculated from Fig.14(A) field and pressure profiles at 19 μsec for m = 1 and k = -2.8 mode.

Fig.18. Typical profiles of B_p, B_t and P at 10.5 μs from start of discharge for high-current case. Estimated poloidal beta β_p = 0.48. Arrow shows magnetic axis calculated from Shafranov formula.

Fig.19. Time history of one-turn voltage. (A) High-current case with peak current of 110 kA; (B) Reduced-current case with peak current of 90 kA.

TABLE 1

	Low current	High current
Major radius R (cm)	12	
Minor radius a (cm)	4.2	
Aspect ratio of torus	2.86	
Radius of conducting shell (cm)	4.75	
Bias field (G)	480	2800
Peak toroidal field (B_t) at plasma center (kG)	5	8
Peak plasma current I_p(kA)	58	110
Maximum current density ($kA \cdot cm^{-2}$)	4	6
Mean current density ($kA \cdot cm^{-2}$)	2	4
Pinch ratio θ	1.5-2.6	1.2-1.6
Time of ionization phase (μsec)	7	2.5
Time of screw pinch (μsec)	2.4	2.4
Time of setting-up phase (μsec)	3.6	5.3
Gas	D_2 (20-50 mtorr)	D_2 or D_2+H_e(10%)

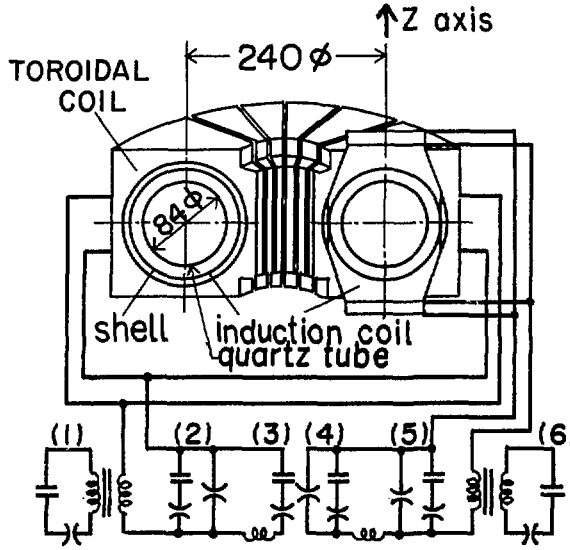
Z axis
240φ
TOROIDAL COIL
84φ
shell
induction coil
quartz tube
(1)
(2)
(3)
(4)
(5)
(6)
(1) POWER CROWBAR BANK 10kV 10kJ
(2) TOROIDAL FIELD BANK 20kV 4kJ
(3) BIAS FIELD BANK 5kV 5kJ
(4) PRE HEATING BANK 20kV 2kJ
(5) PLASMA CURRENT BANK 20kV 10kJ
(6) POWER CROWBAR BANK 10kV 16kJ

Fig. 1

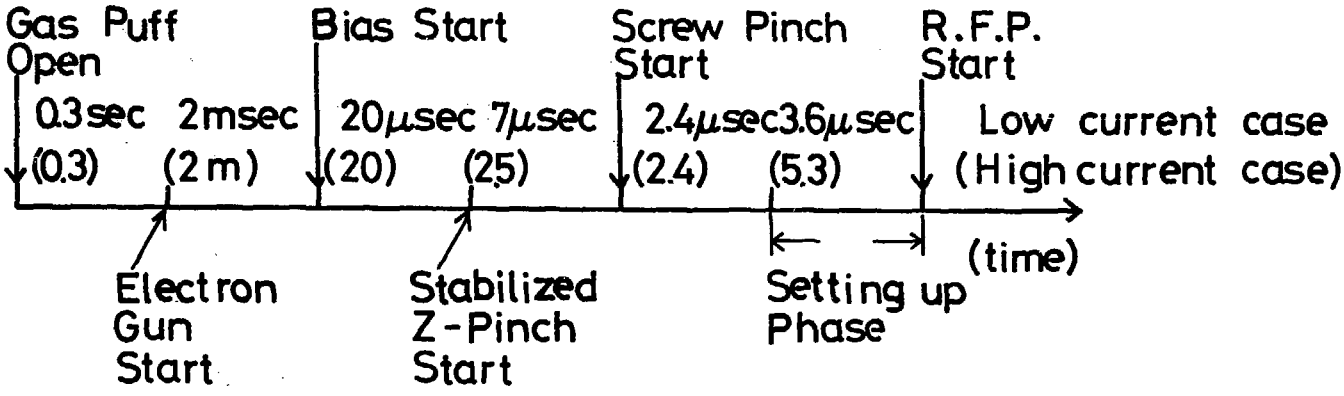
Gas Puff Open
Bias Start
Screw Pinch Start
R.F.P. Start
0.3sec
2msec
20μsec
7μsec
2.4μsec
3.6μsec
Low current case
(High current case)
(0.3)
(2m)
(20)
(25)
(2.4)
(5.3)
(time)
Electron Gun Start
Stabilized Z-Pinch Start
Setting up Phase

Fig.2

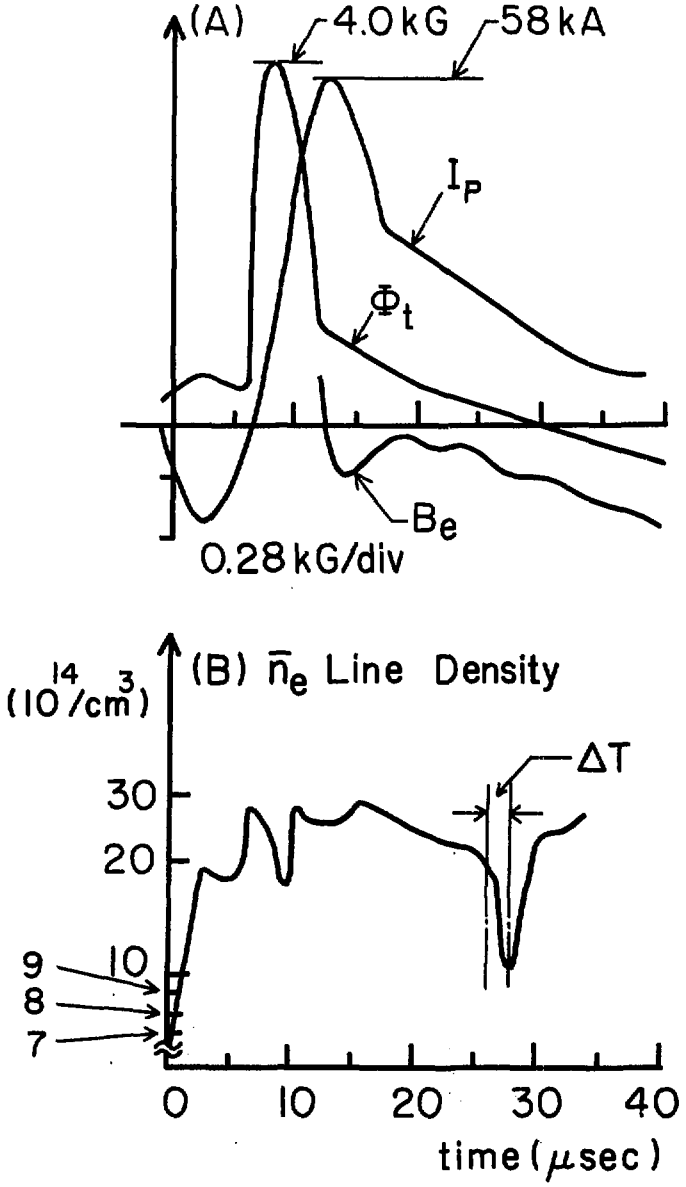
(A)
4.0kG
58kA
I_P
Φ_t
B_e
0.28kG/div
(B) $\bar{n}_e$ Line Density
$(10^{14}/cm^3)$
ΔT
30
20
10
9
8
7
0
10
20
30
40
time (μsec)

Fig.3

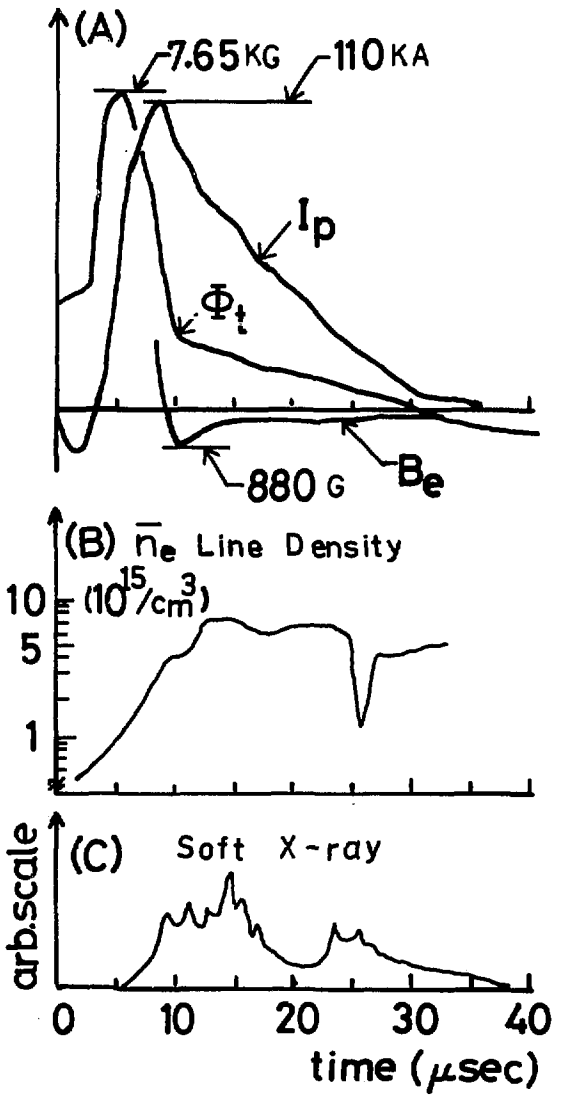
(A)
7.65KG
110KA
Ip
Φt
880 G
Be
(B) n̄e Line Density
(10^15/cm^3)
10
5
1
(C) Soft X-ray
arb.scale
0
10
20
30
40
time (μsec)

Fig.4

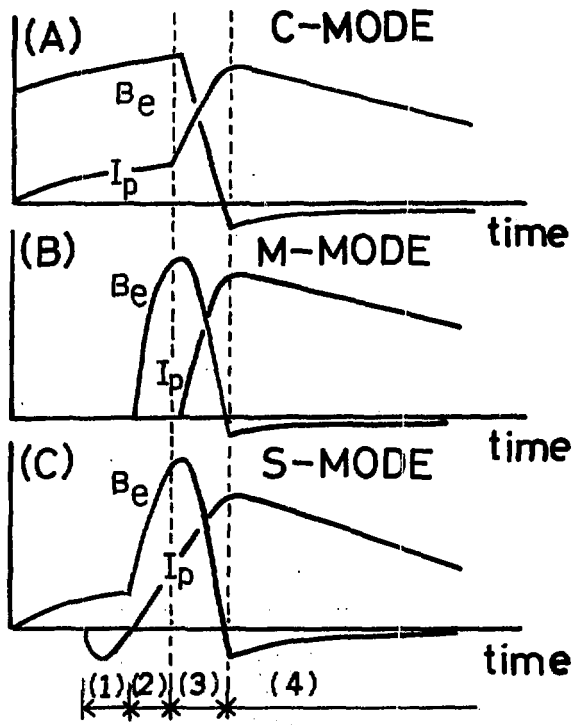

Fig.5

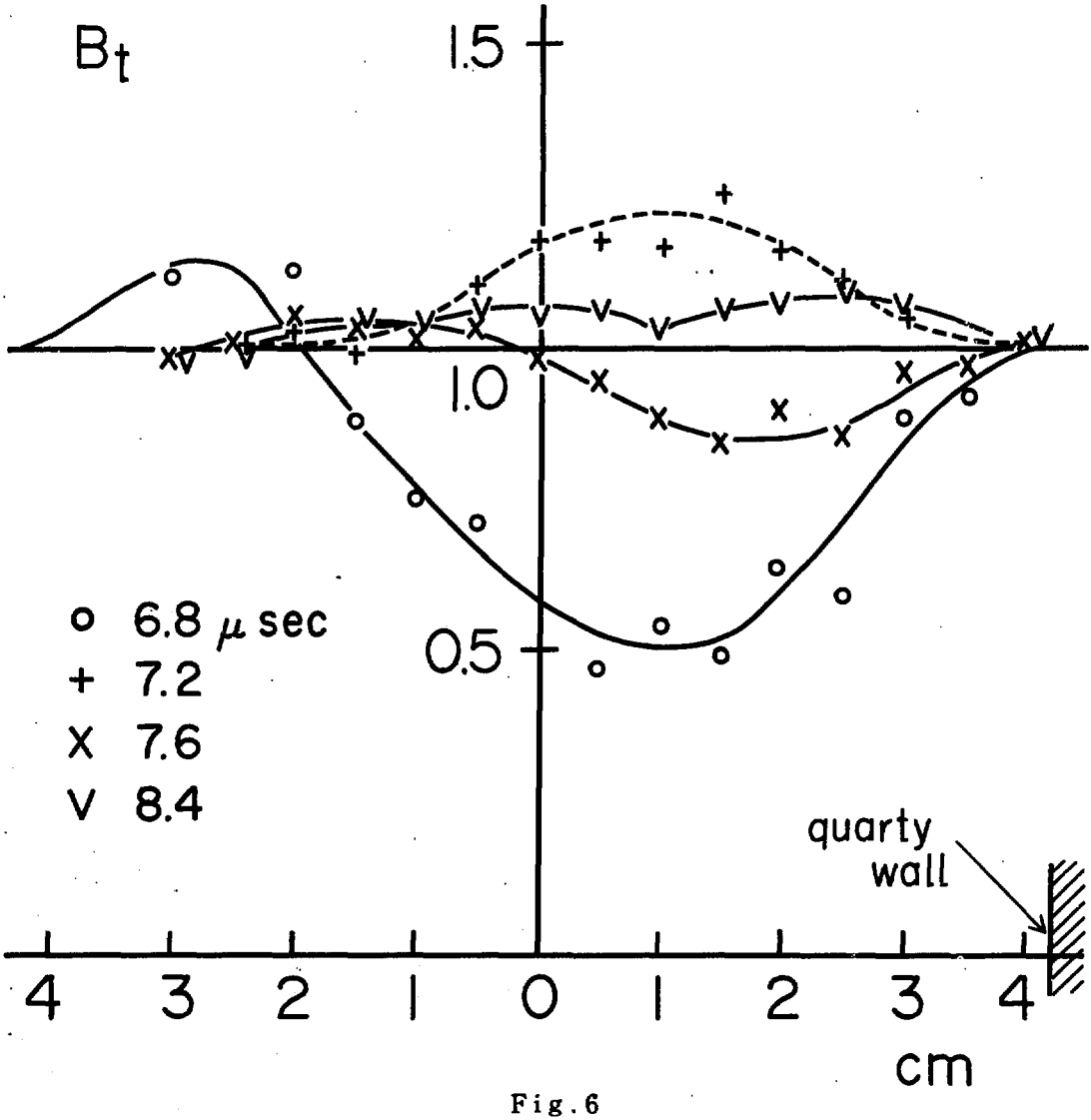

Fig.6

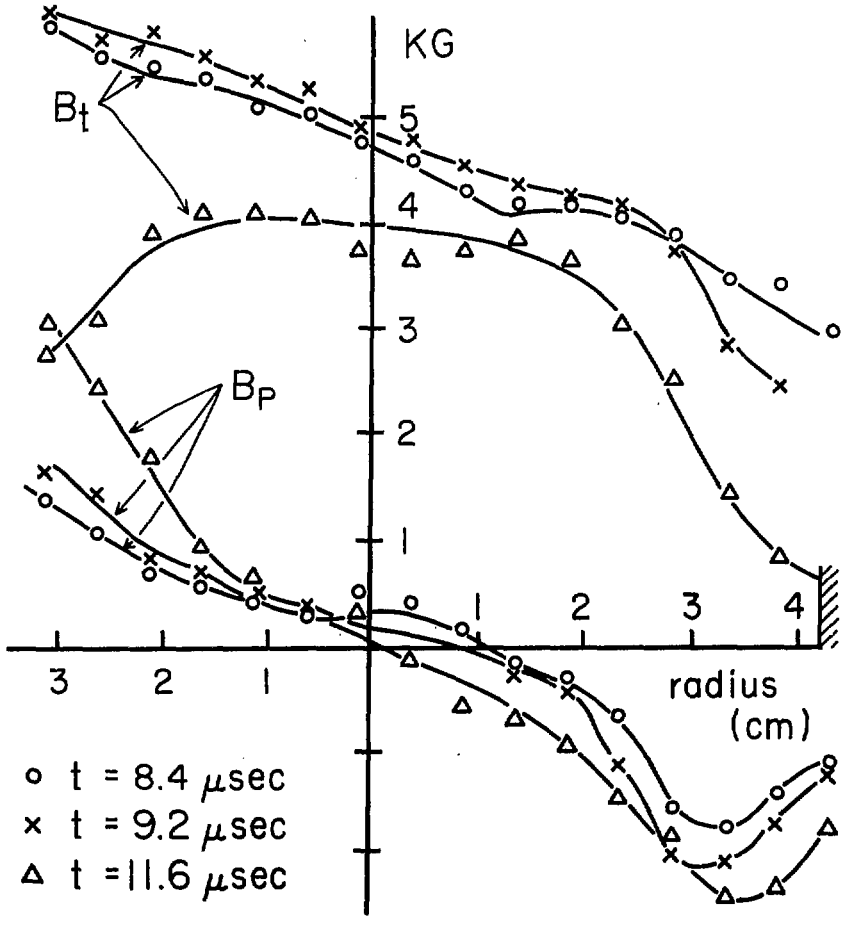

Fig.7

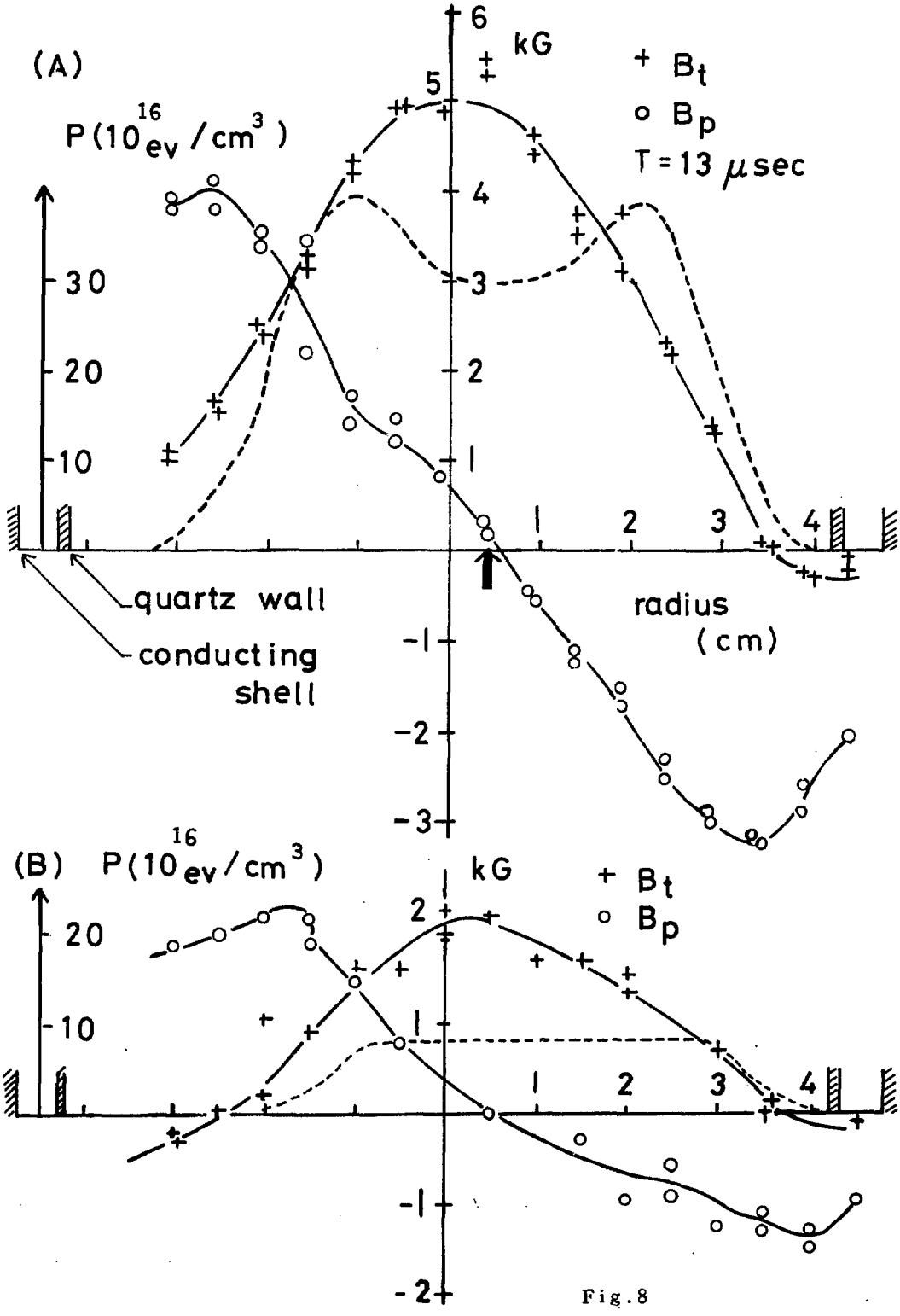
(A)
P(10^16 ev/cm^3)
kG
+ Bt
o Bp
T = 13 μsec
6
5
4
3
2
1
-1
-2
-3
30
20
10
1
2
3
4
quartz wall
conducting shell
radius (cm)
(B) P(10^16 ev/cm^3)
kG
+ Bt
o Bp
20
10
2
1
-1
-2
1
2
3
4

Fig.8

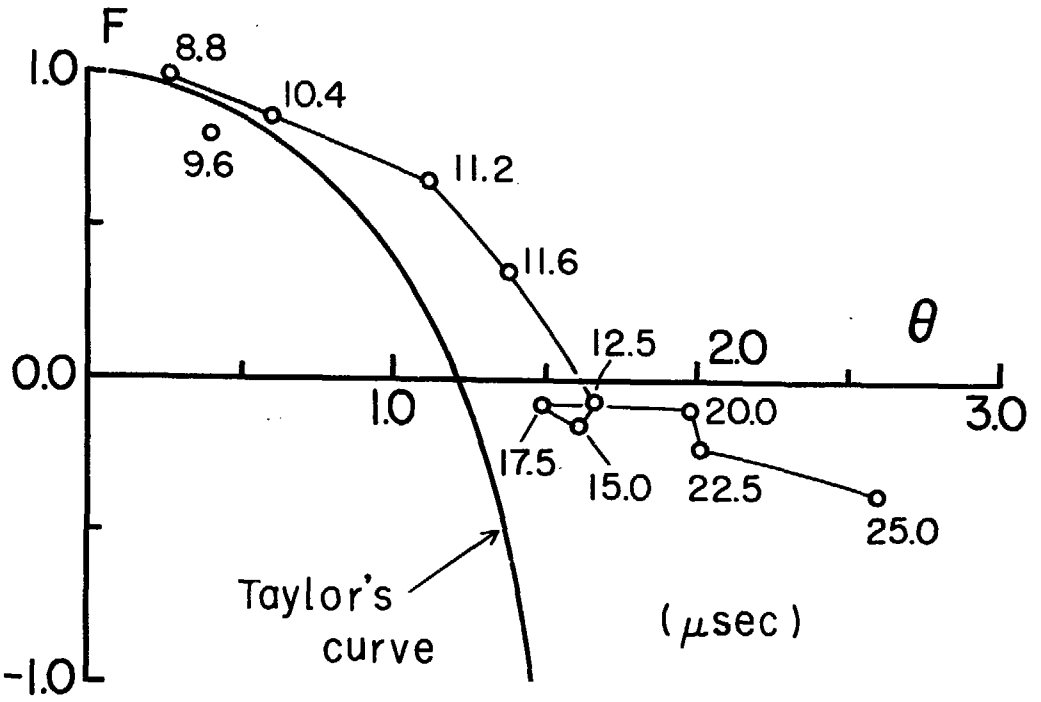
F
1.0
0.0
-1.0
8.8
10.4
9.6
11.2
11.6
12.5
2.0
θ
1.0
3.0
20.0
17.5
15.0
22.5
25.0
Taylor's
curve
(μsec)

Fig. 9

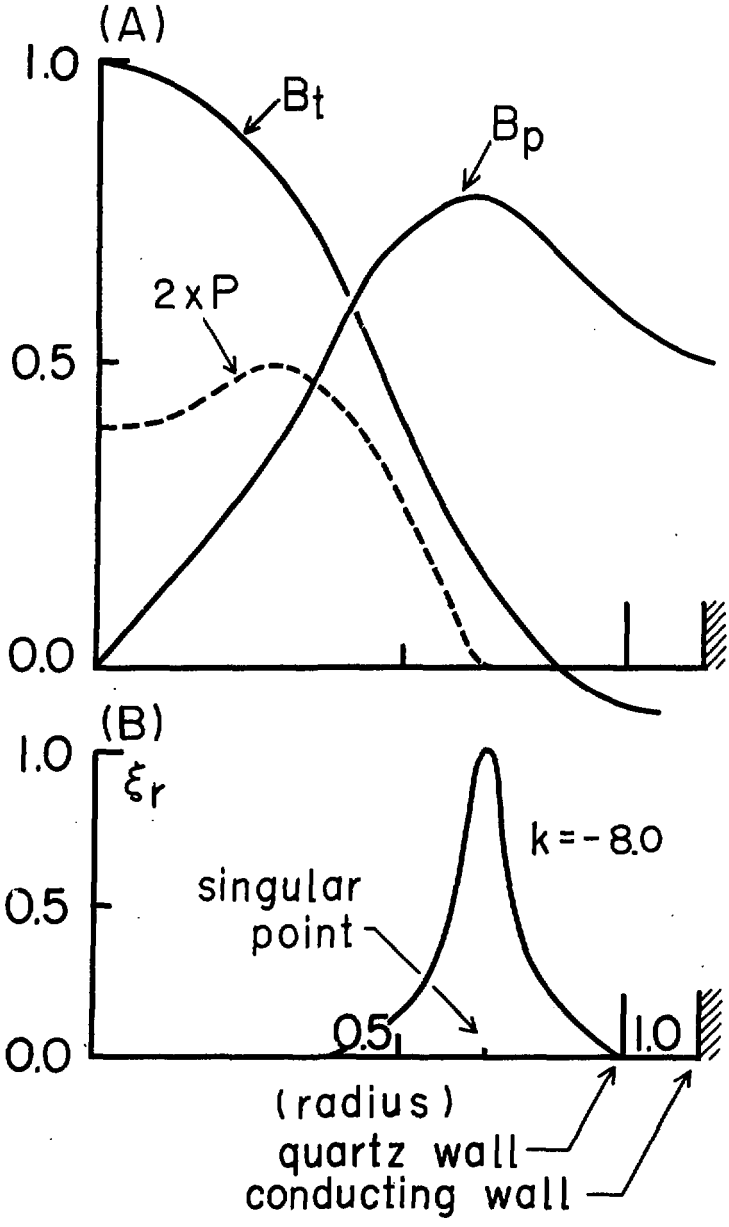
(A)
1.0
0.5
0.0
Bt
Bp
2xP
(B)
1.0
0.5
0.0
ξr
k=-8.0
singular
point
0.5
1.0
(radius)
quartz wall
conducting wall

Fig.10

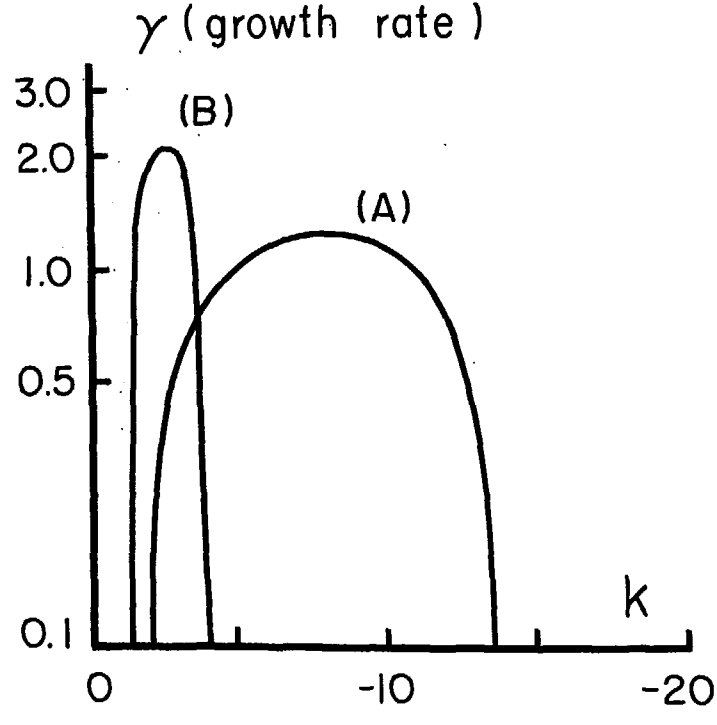
γ (growth rate)
3.0
2.0
1.0
0.5
0.1
(B)
(A)
k
0
-10
-20

Fig. 11

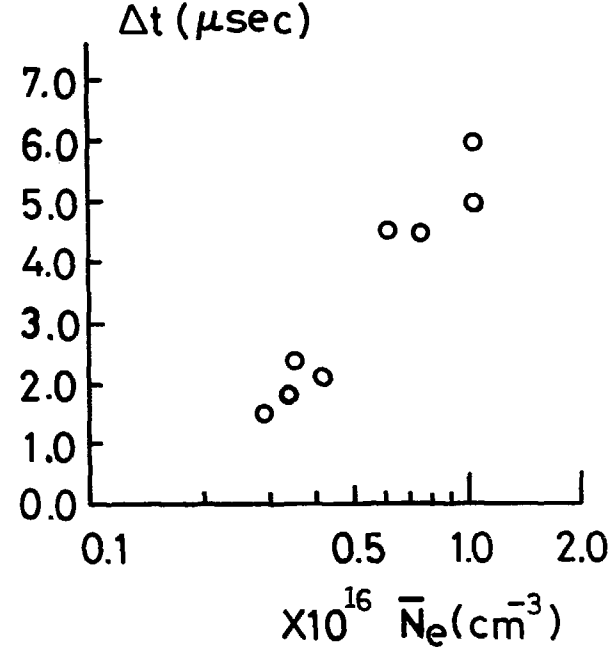
Δt (μsec)
7.0
6.0
5.0
4.0
3.0
2.0
1.0
0.0
0.1
0.5
1.0
2.0
X10^16 N̄e(cm^-3)

Fig. 12

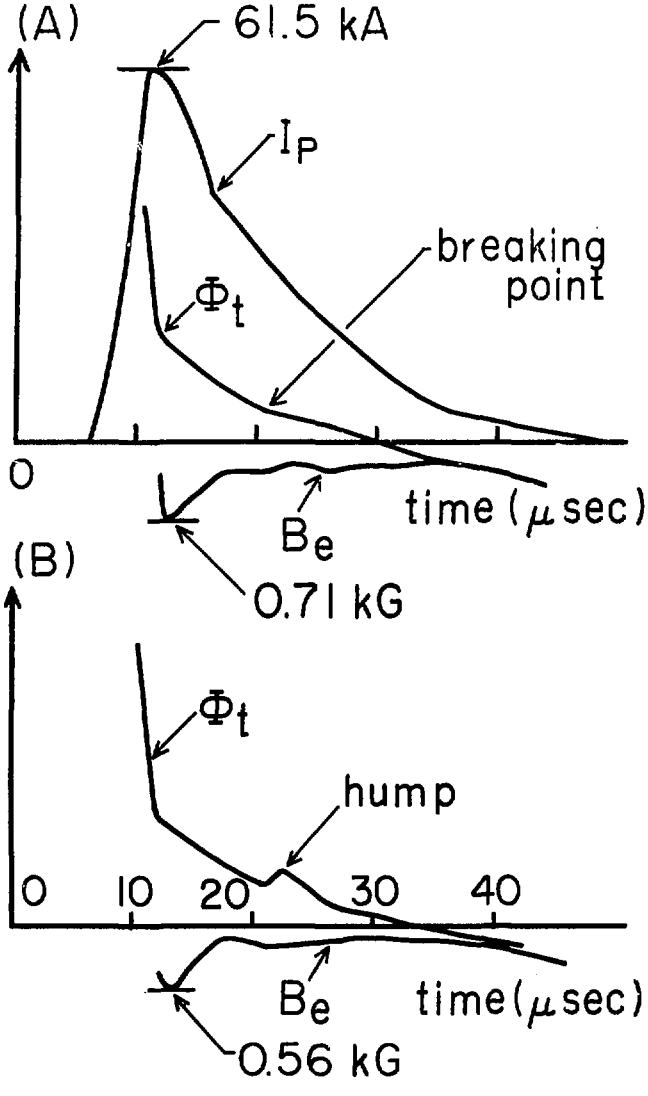
(A)
61.5 kA
I_P
breaking point
Φ_t
0
time (μsec)
B_e
0.71 kG
(B)
Φ_t
hump
0
10
20
30
40
B_e
time(μsec)
0.56 kG

Fig. 13

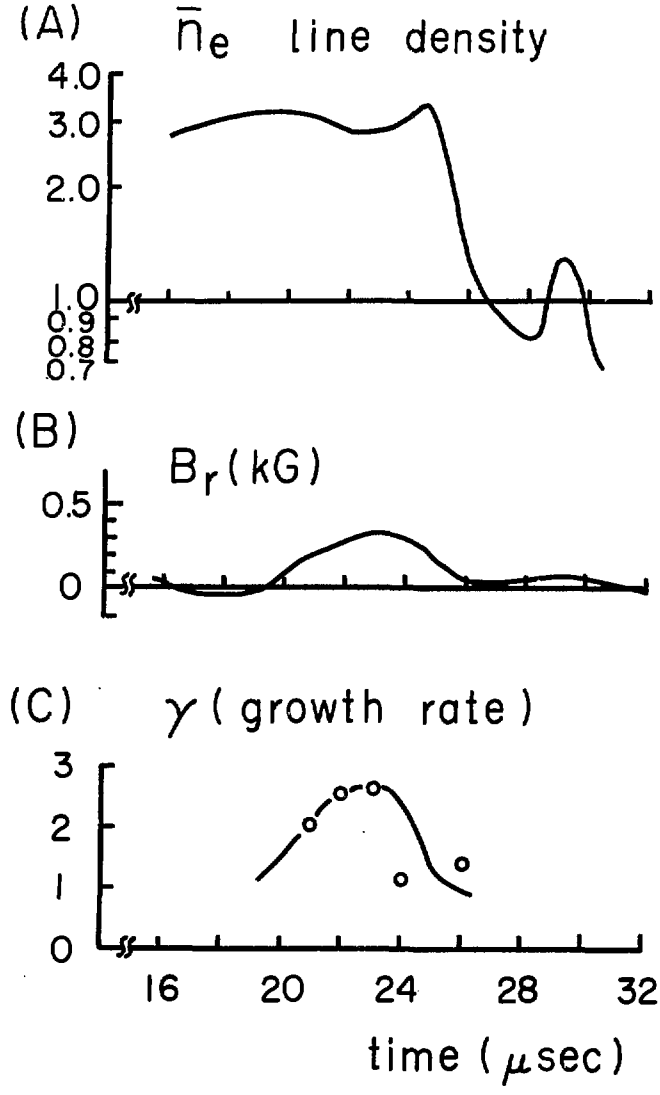
(A)
$\bar{n}_e$ line density
4.0
3.0
2.0
1.0
0.9
0.8
0.7
(B)
B_r (kG)
0.5
0
(C)
γ (growth rate)
3
2
1
0
16
20
24
28
32
time (μsec)

Fig. 14

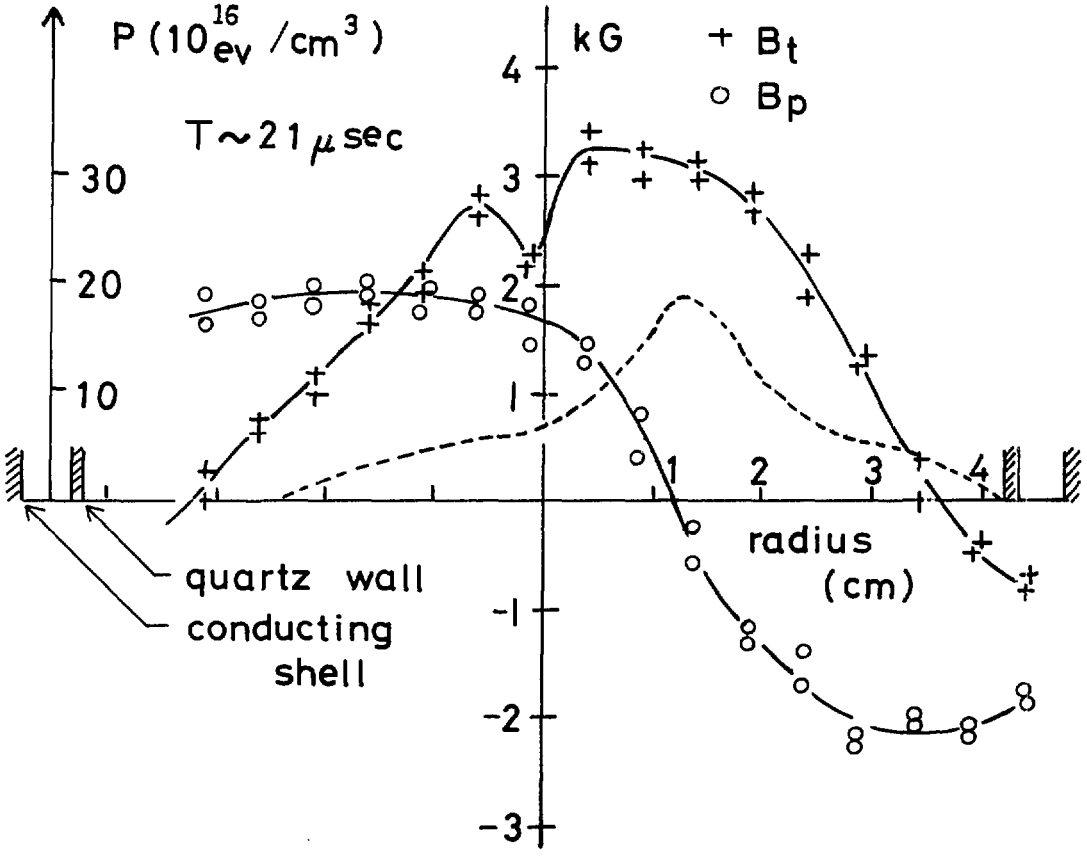
P (10^{16}_{ev} /cm^3)
T~21 μsec
30
20
10
kG
+ Bt
o Bp
4
3
2
1
-1
-2
-3
1
2
3
4
radius
(cm)
quartz wall
conducting
shell

Fig.15

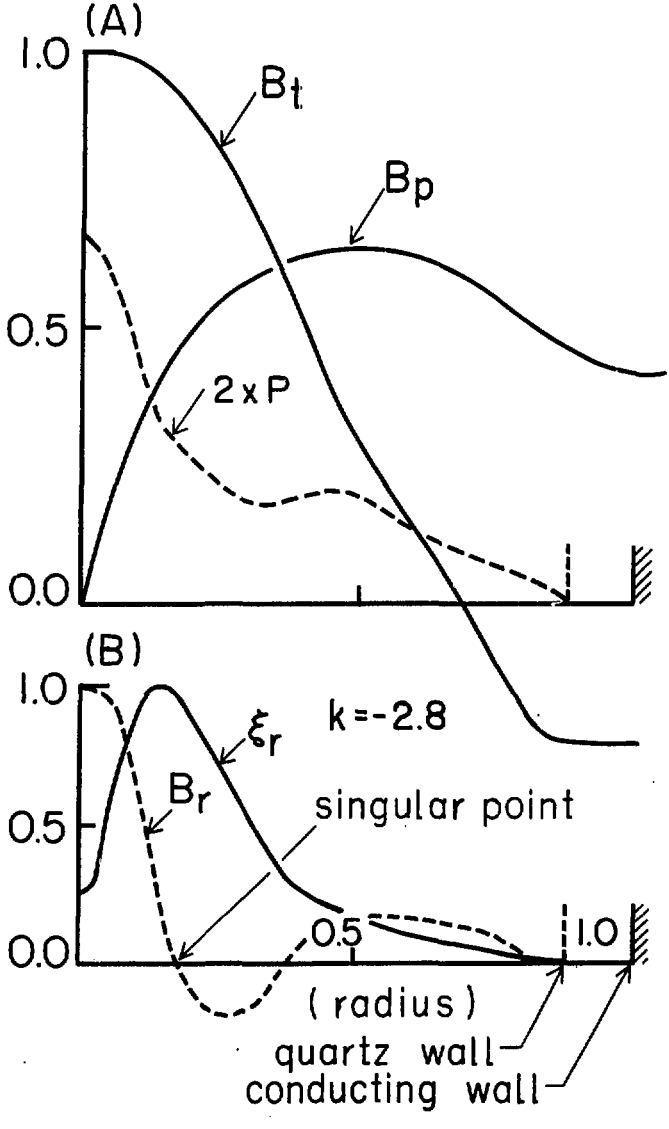
(A)
1.0
0.5
0.0
B_t
B_p
2xP
(B)
1.0
0.5
0.0
ξ_r
k=-2.8
B_r
singular point
0.5
1.0
(radius)
quartz wall
conducting wall

Fig.16

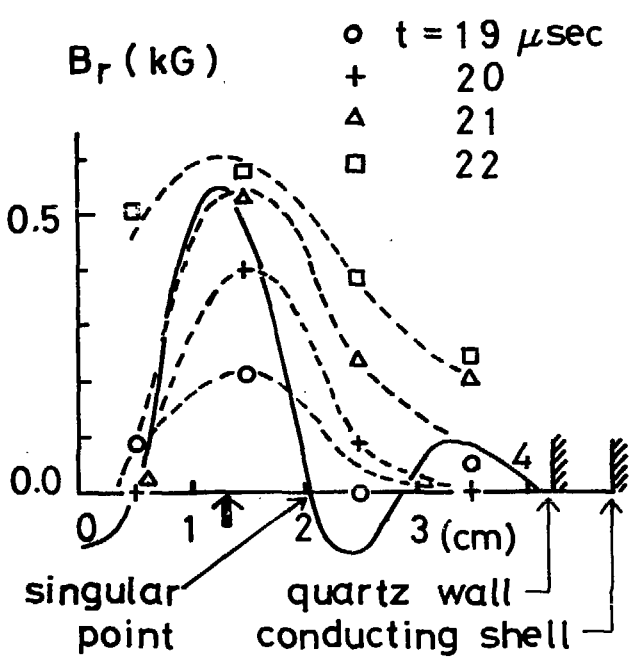
B_r (kG)
o t = 19 μsec
+ 20
△ 21
□ 22
0.5
0.0
0
1
2
3 (cm)
4
singular point
quartz wall
conducting shell

Fig.17

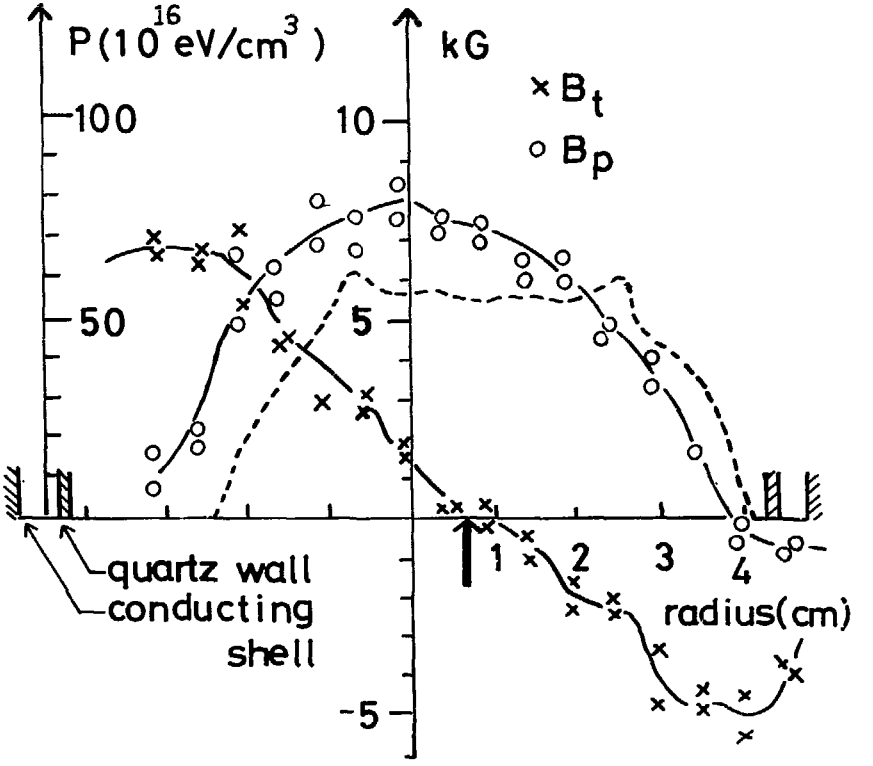
P(10^{16} eV/cm^3)
kG
× B_t
○ B_p
100
50
10
5
-5
quartz wall
conducting shell
1
2
3
4
radius(cm)

Fig.18

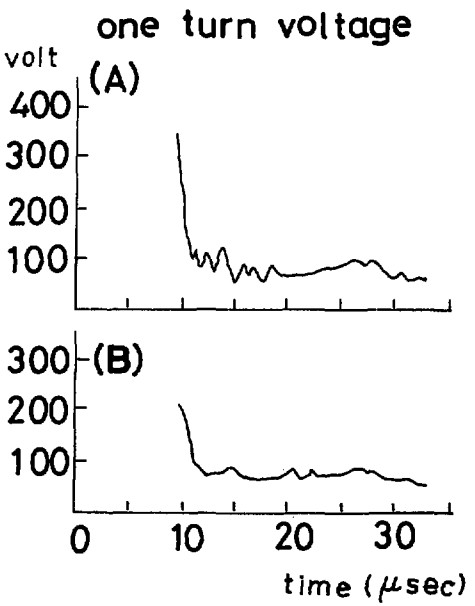
one turn voltage
volt
(A)
400
300
200
100
300
(B)
200
100
0
10
20
30
time (μsec)

Fig. 19